Applied Catalysis B: Environmental 221 (2018) 413–421

Contents lists available at ScienceDirect

Applied Catalysis B: Environmental

journal homepage: www.elsevier.com/locate/apcatb

Research Paper

The insights into chlorine doping effect on performance of ceria supported nickel catalysts for selective CO methanation

M.V. Konishcheva[a,b], D.I. Potemkin[a,b,*], P.V. Snytnikov[a,b], O.A. Stonkus[a], V.D. Belyaev[a], V.A. Sobyanin[a,*]

[a] Boreskov Institute of Catalysis, Pr. Lavrentieva, 5, Novosibirsk, 630090, Russia
[b] Novosibirsk State University, Pirogova St., 2, Novosibirsk, 630090, Russia

ARTICLE INFO

Keywords:
Hydrogen-rich gas
Reformate
Selective or preferential CO methanation
CO cleanup
Nickel ceria catalysts
Effect of chlorine doping
Cerium oxychloride

ABSTRACT

Selective CO methanation (CO-SMET) in the reformate gas, containing (vol.%): 1.0 CO, 65H_2, 10H_2O, 20 CO_2 with He as balance, was investigated over a number of nickel-ceria catalysts: treated with NH_4Cl before (Ni/CeO_2(Cl*)) and after (Ni(Cl*)/CeO_2) Ni deposition, prepared by Cl-containing Ni precursor (Ni(Cl)/CeO_2) and Cl-free one (Ni/CeO_2). The effect of residual chlorine, originating from the catalyst preparation procedures, on the activity and CO selectivity of the samples was demonstrated. It was shown that all Cl-containing Ni/CeO_2 catalysts provided efficient CO cleanup. They provided the removal of CO from reformate gas to the level below 10 ppm with a selectivity up to 90%. The catalyst characterization by BET, XRD, XPS, HAADF-STEM, EDX-mapping, FTIR *in situ* and CO chemisorption techniques revealed that the decrease in chlorine content in the order Ni(Cl)/CeO_2 ≥ Ni(Cl*)/CeO_2 > Ni/CeO_2(Cl*) was accompanied by the increase of Ni dispersion that most likely provided high performance of Ni/CeO_2(Cl*) in CO-SMET. The turnover frequencies of Ni surface atoms as well as activation energies in CO methanation were practically similar for all studied catalysts, indicating that Cl did not influence catalyst's activity and CO methanation proceeded by similar ways over Ni surface in both Cl-free and Cl-containing samples. The advanced performance of Cl-containing catalysts was associated with the inhibition of undesirable side reaction of CO_2 methanation. The chlorine doping effect was attributed to the blockage of surface Ce^{3+}-coupled oxygen vacancy sites by CeOCl species that inhibited ceria-assisted CO_2 activation and hydrogenation. The CeO_2 treatment with NH_4Cl before Ni deposition allows to prepare highly active and selective CO-SMET catalyst with high nickel dispersion and Cl-modified ceria surface.

1. Introduction

Fuel cells with proton exchange membrane (PEMFC) using hydrogen as a fuel are under extensive development in the last few decades. Most often they are considered as an alternative clean energy power sources for different applications [1,2]. A huge amount of work performed by different research groups has been devoted to studying the problem of hydrogen-rich gas production for PEMFC. Hydrogen-rich gas can be produced by steam reforming, partial oxidation or autothermal reforming of hydrocarbons or oxygenated organic compounds, followed by water-gas shift reaction. Besides hydrogen, the product gas mixture (reformate) contains (vol.%): *ca.* 20 CO_2, *ca.* 10 H_2O and 0.5–2.0 CO. Carbon monoxide, being a PEMFC anode poison, must be removed to the level below 10 ppm. CO selective methanation (CO-SMET), also called CO preferential methanation, is one of the promising methods for CO removal from hydrogen-rich gas mixtures (reformate) [3,4]. Due to high CO_2 content in the reformate, the target reaction of CO methanation (1) is accompanied by side reactions of CO_2 methanation (2) and reverse water-gas shift reaction (3), causing considerable consumption of hydrogen and increasing CO outlet concentration:

$$CO + 3H_2 = CH_4 + H_2O;\ \Delta H^\circ = -206\ kJ/mol \quad (1)$$

$$CO_2 + 4H_2 = CH_4 + 2H_2O;\ \Delta H^\circ = -165\ kJ/mol \quad (2)$$

$$CO_2 + H_2 = CO + H_2O;\ \Delta H^\circ = 41\ kJ/mol \quad (3)$$

Therefore, a highly active and selective CO methanation catalyst is needed.

Supported Ru [5–14] and Ni [6,15–20] based system are proposed as a selective CO methanation catalysts. A number of support materials, such as Al_2O_3 [6–9,13–17], TiO_2 [5,6,10,12,20], SiO_2 [6,15], MgO [6,15], CeO_2 [17–19], ZrO_2 [6,17] and zeolite [7,14], are used for

* Corresponding authors at: Novosibirsk State University, Pirogova St 2, Novosibirsk 630090, Russia.
E-mail addresses: potema@catalysis.ru (D.I. Potemkin), sobyanin@catalysis.ru (V.A. Sobyanin).

http://dx.doi.org/10.1016/j.apcatb.2017.09.038
Received 13 July 2017; Received in revised form 14 September 2017; Accepted 16 September 2017
Available online 20 September 2017
0926-3373/

preparation of the catalysts. The metal loading, crystallite size [9–12] and the nature of the support [6,12,14,15] were found to be an important factors controlling the overall catalyst performance and selectivity. As shown in recent review [21], chloride residues on the catalyst surface is of key importance for the performance of Ru- and Ni-containing catalysts in CO-SMET reaction. In the most cases, appropriate amount of chlorine dramatically inhibited the CO_2 hydrogenation activity and promoted CO selectivity [8,16,20–22]. The authors of [16] studied CO-SMET over Ni/Al_2O_3 and by combined FTIR and CO_2-TPD measurements showed that chlorine adsorbed on Ni diminished the formation of CO_2-derived carboxylate species on Ni-metal sites and thereby promoted reaction selectivity. In Ref. [20] it was reported that, in the case of Ni/TiO_2 catalysts, a trace amount of Cl at the interface of Ni and TiO_2 improves the selectivity. They also mentioned that when Cl was removed from the Ni/TiO_2 catalyst, selectivity decreased significantly. Such a situation is typical for chlorine which is known as a conventional catalyst selectivity promoter (*e.g.* ethylene epoxidation) [23,24]. However, despite recent studies the origin of chlorine doping effect on the CO-SMET performance is not yet fully cleared.

Recently, we have shown that Ni/CeO_2 catalysts prepared with the use of Ni(II) chloride as Ni precursor [18,19,22] had high selectivity and were able to reduce CO concentration in CO-SMET in the presence of CO_2 to a level of 10 ppm. Catalyst stability was confirmed for at least 70 h [18]. The CO_2 methanation was inhibited due to the formation of surface CeOCl species on ceria surface. However, Ni/CeO_2 prepared with the use of Ni(II) chloride precursor was less active than Ni/CeO_2 prepared with the use of Ni(II) nitrate precursor [18,19,22]. The Cl-free Ni/CeO_2 catalyst was active in both CO and CO_2 methanation. So, there is a task to optimize the chlorine doping procedure to provide high Ni dispersion over Cl-containing ceria in order to obtain highly active and selective catalyst.

In the present paper we critically analyzed our previous results and compared them with new data in order to clarify how does the chlorine doping procedure influence the structure and catalytic properties in CO-SMET of nickel-ceria catalysts. We considered three principal opportunities: Cl doping before and after Ni deposition and the use of Cl-containing Ni precursor. The Cl-free Ni/CeO_2 catalyst was also considered. The correlations between the catalyst performance in CO-SMET and catalyst characterization data by BET, XRD, XPS, HAADF-STEM, EDX-mapping, FTIR *in situ* and CO-chemisorption techniques as well as the origin of chlorine promotion effect are discussed.

2. Experimental

2.1. Materials

$Ce(NO_3)_3{\cdot}6H_2O$ (99%, Novosibirsk factory for rare earth), $Ni(NO_3)_2{\cdot}6H_2O$ (99%, Reachim Russia) $NiCl_2{\cdot}6H_2O$ (99.9%, Sigma-Aldrich), NH_4Cl (99%, Reachim Russia) were used for catalyst preparation. CO_2 gas was passed through carbon filter, CO was treated in quartz column operated at 150 °C to clean it out from possible Fe carbonyls contamination before addition to reaction mixture. All other chemicals were commercially purchased and used without additional purification.

2.2. Catalyst preparation

The ceria supported nickel catalysts (represented below as Ni/CeO_2, $Ni(Cl)/CeO_2$, $Ni(Cl^*)/CeO_2$ and $Ni/CeO_2(Cl^*)$) were prepared by incipient wetness impregnation method. The CeO_2 support was produced by the calcinations of cerium(III) nitrate in air for 2 h at 400 °C.

The Cl-free Ni/CeO_2 catalyst was prepared by impregnating CeO_2 with an aqueous solution of Ni(II) nitrate followed by drying in air at 110 °C and reduction in the 5 vol.% H_2/He flow at 400 °C. The Cl-containing $Ni(Cl)/CeO_2$ catalyst was prepared by similar way using Ni (II) chloride as a precursor.

The Cl-containing $Ni(Cl^*)/CeO_2$ catalyst was prepared by impregnating Cl-free Ni/CeO_2 catalyst with an aqueous solution of ammonium chloride (NH_4Cl) followed by drying in air at 110 °C and reduction in the 5 vol.% H_2/He flow at 400 °C.

The $Ni/CeO_2(Cl^*)$ catalyst was prepared by impregnating the chlorine-doped ceria $CeO_2(Cl^*)$ with an aqueous solution of Ni(II) nitrate followed by drying in air at 110 °C and reduction in the 5 vol.% H_2/He flow at 400 °C. The chlorine doped ceria $CeO_2(Cl^*)$ was prepared by impregnation of CeO_2 with an aqueous solution of ammonium chloride followed by drying in air at 110 °C and reduction in the 5 vol. % H_2/He flow at 400 °C.

Note that the calculated content of nickel in the catalysts was 8–10 wt.%, that of chlorine in the chlorinated samples was *ca.* 12 wt.% excluding losses during catalysts reduction. For $Ni(Cl^*)/CeO_2$ and $Ni/CeO_2(Cl^*)$ catalysts the quantity of introduced NH_4Cl was adjusted to be equimolar to the quantity of chlorine used in the case of $Ni(Cl)/CeO_2$ catalyst. All catalysts after reduction at 400 °C were cooled in 5 vol.% H_2/He flow to ambient temperature. Then H_2/He gas mixture was purged out by flowing He and the He atmosphere was substituted by air. The obtained catalyst powders were pressed into pellets, crushed, and the 0.1–0.2 mm particle size fraction was separated and used in catalytic experiments.

2.3. Catalyst characterization

The Ni loading of the catalysts was determined by inductively coupled plasma atomic emission spectrometry (an Optima instrument).

The chlorine content in the samples was determined by atomic-absorption spectrometry (Hitachi Z-8000 instrument) as described in [25].

The specific BET surface area (S_{BET}) of the catalysts was determined from the complete nitrogen adsorption isotherms at −196 °C (ASAP 2400 instrument). Prior to the measurements samples were evacuated at 150 °C for 2 h.

The XRD, HAADF-STEM, EDX-mapping, XPS, FTIR *in situ* and CO chemisorption techniques were applied to characterize the used catalysts after *ca.* 100 h on stream, including *ca.* 20 h on reformate stream.

The XRD patterns were obtained on a Bruker D8 Advance diffractometer (Cu Kα radiation) equipped with a LynxEye position sensitive detector. The measurements were carried out in the 2θ range of 20°–80° with a step of 0.02°. The ICDD PDF-2 database was used for phase identification. The Rietveld refinement with quantitative phase analysis was performed using TOPAS v4.2 software. The sizes of the coherent scattering regions (D_{XRD}) were calculated by the line broadening analysis according to the Scherrer equation.

The high-angle annular dark-field scanning TEM (HAADF-STEM) analysis was performed using a 200 kV JEM-2200FS electron microscope. The scanning mode was employed together with EDX spectroscopy. The samples for the study were prepared on a holey carbon film mounted on a copper grid.

X-Ray photoelectron spectroscopy (XPS) was applied to determine surface composition of the used catalysts, which however had contacted with ambient air before they were moved to spectrometer. The XPS measurements were carried out using a KRATOS ES 300 spectrometer with Mg K_α irradiation. The XP-spectra were registered at low power of the X-ray gun (10 kV × 5 mA, 50 W power) in order to prevent X-ray damage of the ceria surface. The spectra were calibrated by Ce3d U'" line with binding energy of 916.7 eV. The XP spectra were processed with WinCalc software. The Shirley-model was used for subtraction of the inelastic photoelectron background. The spectra were fitted by Gauss–Lorentz functions. The% of Gauss-Lorentz distribution was chosen individually for each spectrum for better fitting. However, it was close to 50%.

The nature of surface species during the CO_2 methanation over the catalysts was studied by the Fourier transform infrared spectroscopic (FTIR) *in situ* technique. IR spectra (64 scans per spectrum, resolution

4 cm^{-1}) were acquired with a Shimadzu IRAffinity-1 spectrometer. A Harrick High Temperature Cell equipped with KBr windows was used for the studies. The catalysts were pressed into disks of 13 mm diameter and 25 mg weight. Before being studied, the catalysts were reduced in H_2/He flow at 350 °C for 1 h, cooled to 250 °C and background spectra were acquired. Then the reaction mixture (vol.% 1 CO_2 + 65H_2 + He-balance) was fed and spectra at 250 °C were acquired again. In order to provide uniform reaction conditions for the whole sample disk WHSV was adjusted to 168,000 $cm^3\ g_{cat}^{-1}\ h^{-1}$ and therefore the CO_2 conversion was below 30%. The spectra were acquired in every 2–3 min during half an hour interval until they kept constant. The resulting spectra are presented after correction for background and subtraction of spectra of gaseous CO_2.

Dispersion of supported Ni was evaluated using the data on pulse chemisorption of CO in H_2 at 20 °C, assuming that each surface Ni atom adsorbs one CO molecule. CO adsorption over pure CeO_2 was negligible. Prior to the CO chemisorption measurements, the catalysts were reduced in the hydrogen flow at 350 °C for 0.5 h. The technique of pulse titration of the Ni surface was similar to that described elsewhere [26]. The specific surface area and mean size of the supported Ni particles were determined using the chemisorption results.

2.4. Catalytic activity measurements

The reaction of CO-SMET was performed in a fixed-bed continuous-flow quartz reactor (i.d.: 3 mm, catalyst bed length: 28 mm) at atmospheric pressure. In all experiments, 0.25 g of the catalyst (partial size of 0.1–0.2 nm) was placed in the reactor. The temperature was measured by a K-type thermocouple in the middle of the catalyst bed. The experiments were performed with the following feed gas composition (vol.%): 1.0 CO, 65H_2, 10H_2O, 20 CO_2 with He as balance; and at WHSV of 29,000 $cm^3\ g^{-1}\ h^{-1}$.

To prevent the formation of volatile $Ni(CO)_4$, which is thermodynamically feasible at temperatures < 150 °C, the catalytic experiments were performed in the temperature interval of 180–360 °C. Initially, the reactor with catalyst was heated to 170 °C in He flow, then the reaction mixture was fed to the reactor upon continuous heating to 360 °C; after that the reactor was cooled to 180 °C and catalytic experiments were started. Each catalyst was tested in several cycles of temperature increasing/decreasing. Temperature was increased/decreased stepwise with time of stay at each point of 20 min and ramp speed of 3 °C/min. Catalytic characteristics of all samples were reproducible and stable for at least 20 h. The stability of Ni/CeO_2(Cl*) catalyst was confirmed after 120 h on stream (See Fig. S6 in Supplementary information).

The inlet and outlet concentrations were determined online using a Chromos GC-1000 gas-chromatograph equipped with Porapak Q column and a flame-ionization (FID) detector. The combination of a methanator (containing a reduced nickel catalyst) and the FID allowed highly sensitive analysis of CO, CO_2, and hydrocarbons in the gas mixture. The detection limit of the CO, CH_4, and CO_2 was 0.5 ppm. Methane was the main reaction product. Small amounts of ethane (< 0.01 vol.%) were detected for Ni/CeO_2 catalyst.

The catalyst performance was characterized by the CO outlet concentrations ($[CO]_{out}$), CO selectivity (S_{CO}) and conversions of CO (X_{CO}) and CO_2 ($X_{CO_2}^{Ref}$) which were calculated by the following equations:

$$S_{CO}(\%) = \frac{F_{CO}^{in} - F_{CO}^{out}}{F_{CH_4}^{out}} \cdot 100, \quad (4)$$

$$X_{CO}(\%) = \frac{F_{CO}^{in} - F_{CO}^{out}}{F_{CO}^{in}} \cdot 100, \quad (5)$$

$$X_{CO_2}^{Ref}(\%) = \frac{F_{CH_4}^{out} - X_{CO} \cdot F_{CO}^{in}}{F_{CO_2}^{in}} \cdot 100, \quad (6)$$

where F_{CO}^{in} and $F_{CO_2}^{in}$ are the inlet molar flow rates of CO and CO_2 (moles/s), F_{CO}^{out} and $F_{CH_4}^{out}$ are the outlet molar flow rates of CO and CH_4 (moles/s), respectively.

The CO and CO_2 methanation activity of the catalysts at CO-SMET were also characterized by turnover frequencies (TOF) of the Ni surface atoms. The TOFs of the Ni surface atoms for CO methanation were determined from experimental data obtained at low CO conversion (X_{CO} < 15%) and $S_{CO} \approx 100\%$ for all the catalysts. The TOFs for CO_2 methanation (TOF_{CO2}^{Ref}) were determined from experimental data obtained at low CO_2 conversion (X_{CO2} < 10%). TOF_{CO} and TOF_{CO2}^{Ref} were calculated by the following equations:

$$TOF_{CO}(s^{-1}) = \frac{F_{CH_4}^{out} \cdot N_a}{m \cdot S_{Ni} \cdot N}, \quad (7)$$

$$TOF_{CO2}^{Ref}(s^{-1}) = \frac{F_{CH_4}^{out} \cdot (1 - S_{CO}/100) \cdot N_a}{m \cdot S_{Ni} \cdot N}, \quad (8)$$

where $F_{CH_4}^{out}$ – the outlet molar flow rate of CH_4 (moles/s), N_a – Avogadro's number, m – catalyst weight (g), S_{Ni} – specific surface area of supported metallic Ni particles, calculated from CO adsorption data (m^2/g_{cat}), N – amount of Ni atoms per 1 m^2 of nickel surface area.

To emphasize the differences in catalytic activity towards CO_2 methanation a set of experiments on CO_2 methanation was carried out in a model mixture with the following feed gas composition (vol.%): 1.0 CO_2, 65H_2 with He as balance; and at WHSV of 29 000 $cm^3 g^{-1}\ h^{-1}$. The CO_2 methanation activity of the catalysts was characterized by CO_2 conversion (X_{CO2}) and TOFs of the Ni surface atoms (TOF_{CO2}). TOF_{CO2} were determined from experimental data obtained at low CO_2 conversion (X_{CO2} < 25%). X_{CO2} and TOF_{CO2} were calculated by the following equations:

$$X_{CO2}(\%) = \frac{F_{CO_2}^{in} - F_{CO_2}^{out}}{F_{CO_2}^{in}} \cdot 100, \quad (9)$$

$$TOF_{CO2}(s^{-1}) = \frac{F_{CH_4}^{out} \cdot N_a}{m \cdot S_{Ni} \cdot N}, \quad (10)$$

where $F_{CO_2}^{in}$ is the inlet molar flow rate of CO_2 (moles/s), and $F_{CH_4}^{out}$ are the outlet molar flow rates of CO_2 and CH_4 (moles/s), respectively, N_a – Avogadro's number, m – catalyst weight (g), S_{Ni} – specific surface area of supported metallic Ni particles, calculated from CO adsorption data (m^2/g_{cat}), N – amount of Ni atoms per 1 m^2 of nickel surface area.

3. Results and discussion

3.1. Catalysts characterization

3.1.1. Chemical composition and S_{BET}

Table 1 presents the actual Ni and Cl loadings and specific BET surface area (S_{BET}) of the catalysts.

The nickel loading (7.4–9.7 wt.%) was close to the calculated value

Table 1
Nickel and chlorine loading and SBET of the used catalysts.

Catalyst	Chemical composition[a], wt.%		S_{BET}[c],m^2/g
		Ni[a]	Cl[b]
CeO_2	–	–	100
Ni/CeO_2[d]	7.4	–	88
Ni(Cl*)/CeO_2	7.4	8.0	46
Ni(Cl)/CeO_2[d]	9.7	8.5	56
Ni/CeO_2(Cl*)	7.8	1.5	70

[a]Ni loading determined by inductively coupled plasma atomic emission spectrometry.
[b]Cl loading, determined by atomic–absorption spectrometry.
[c]BET surface area determined by the nitrogen adsorption isotherms at –196 °C.
[d]Adapted from [19].

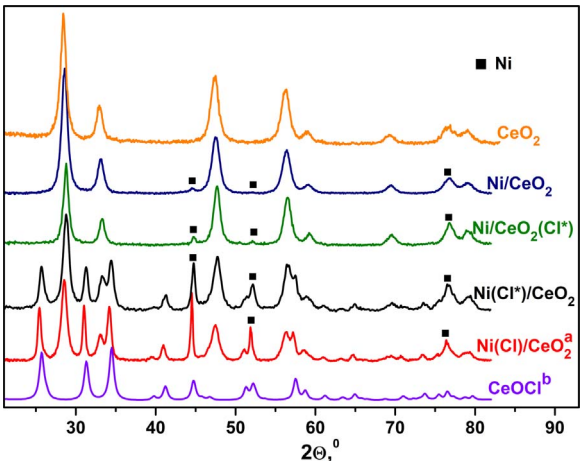

Fig. 1. XRD patterns of samples.
[a]Adapted from [19]; [b]Adapted from ICDD PDF-2 database.

(8–10 wt.%) for all samples. The actual chlorine loading was significantly lower than the calculated value (~12 wt.%) for Cl-containing catalysts. The chlorine loadings in Ni(Cl)/CeO_2 and Ni(Cl*)/CeO_2 were similar (8.5 and 8.0 wt.%, respectively), while Ni/CeO_2(Cl*) contained only *ca.* 1.5 wt.% of chlorine. This most likely means that significant amount of chlorine was lost owing its passing to the gas phase during catalyst preparation.

S_{BET} of Cl-free Ni/CeO_2 (88 m^2/g) was quite similar to that of CeO_2 (100 m^2/g). S_{BET} of Cl-containing Ni(Cl)/CeO_2 (56 m^2/g), Ni(Cl*)/CeO_2 (46 m^2/g) and Ni/CeO_2(Cl*) (70 m^2/g) was much lower than that of CeO_2 and Ni/CeO_2.

Probable reasons for a lower content of chlorine in Ni/CeO_2(Cl*) as compared to Ni(Cl)/CeO_2 and Ni(Cl*)/CeO_2, as well as lower S_{BET} values of chlorinated catalysts as compared to CeO_2 and Ni/CeO_2, are discussed in the next section.

3.1.2. XRD and CO chemisorption

Fig. 1 shows the XRD patterns of CeO_2, CeOCl and the used catalysts. Table 2 presents the obtained data.

The XRD patterns of all samples contain diffraction peaks of CeO_2 (PDF #34-0394), which consists of nanocrystalline particles (size, D_{XRD} ~9.0–9.5 nm) and has the unit cell parameter of 0.5411 nm. The metallic Ni phase (PDF #04-0850) was observed in all catalysts as well. The mass fractions of Ni phase detected by XRD in Ni(Cl*)/CeO_2 and Ni(Cl)/CeO_2 were consistent with the actual Ni loading (Tables 1 and 2), indicating the absence of highly dispersed or amorphous species on the support surface. At the same time, for the Ni/CeO_2 and Ni/CeO_2(Cl*) catalysts, the mass fraction of Ni phase detected by XRD was lower than actual Ni loading (Tables 1, 2). This fact most likely means that Ni exists on the support surface not only as well-crystallized phase, but in a form of highly dispersed or amorphous species as well.

Table 2
XRD and CO chemisorptions data for the used catalysts.

Catalyst	Phase composition[a]	Mass fraction[b], wt.%	D_{XRD}[c],nm	D_{CO}[d],nm	S_{Ni}[e],m^2/g_{cat}
CeO_2	CeO_2	100	9	–	–
Ni/CeO_2[f]	Ni	4	10	13	3.8
	CeO_2	96	9	–	
Ni(Cl*)/CeO_2	Ni	8	30	31	1.7
	CeO_2	50	9.5	–	
	CeOCl	42	14.5	–	
Ni(Cl)/CeO_2[f]	Ni	8	> 100	120	0.5
	CeO_2	50	9.5	–	
	CeOCl	42	19		
Ni/CeO_2(Cl*)	Ni	~5	21	17	3.1
	CeO_2	~95	9	–	

[a,b]Phase composition and phase mass fraction according to XRD data.
[c,d]Average size of Ni particles according to XRD (DXRD) and CO chemisorption (DCO) data.
[e]Ni surface area according to CO chemisorption data.
[f]Adapted from [19].

For the catalysts, the size of the coherent scattering regions of Ni (D_{XRD}) ranged within ~ 10 ÷ 100 nm (Table 2) and followed the trend:

$$Ni/CeO_2 < Ni/CeO_2(Cl^*) < Ni(Cl^*)/CeO_2 < Ni(Cl)/CeO_2$$

Respective Ni particle sizes (D_{CO}) determined by CO chemisorption increase in the same order. Indeed, as Table 2 shows, D_{CO} was close to the D_{XRD} for all the catalysts. Specific surface area of Ni (S_{Ni}) for the catalysts (Table 2) correlates with average Ni particle size. S_{Ni} descended in the range ~ 3.8 ÷ 0.5 m^2/g_{cat} and followed the trend:

$$Ni/CeO_2 > Ni/CeO_2(Cl^*) > Ni(Cl^*)/CeO_2 > Ni(Cl)/CeO_2$$

Besides ceria and nickel phases, Cl-containing Ni(Cl)/CeO_2 and Ni(Cl*)/CeO_2 catalysts (Table 2) contained CeOCl phase with particle sizes D_{XRD} of 19.0 and 14.5 nm, respectively. Formation of CeOCl phase in the chlorinated catalysts is quite expectable, especially in view of works [27–31] which prove that the use of chlorinated precursors for preparation of Pd/CeO_2 and Rh/CeO_2 catalysts leads to the formation of CeOCl phase upon reduction in H_2. Mass fraction of CeOCl phase detected by XRD for Ni(Cl)/CeO_2 and Ni(Cl*)/CeO_2 was ~40 wt.% (Table 2), that corresponded to chlorine content of *ca.* 8 wt.% and was close to actual chlorine loading (Table 1). Thus, the lower S_{BET} of the Ni(Cl)/CeO_2 and Ni(Cl*)/CeO_2 (Table 1) as compared to S_{BET} of CeO_2 and Ni/CeO_2 could be associated with the formation of considerable amount of CeOCl phase, which has a larger crystalline size than that of CeO_2.

The Ni/CeO_2(Cl*) catalyst contained 1.5 wt.% of chlorine, that was much less than chlorine loadings in Ni(Cl)/CeO_2 and Ni(Cl*)/CeO_2 (Table 1). In contrast to other chlorinated catalysts, no CeOCl phase was detected in Ni/CeO_2(Cl*) (Fig. 1 and Table 2). The low chlorine content and the absence of CeOCl phase in Ni/CeO_2(Cl*) may result from the fact that the catalyst was prepared by chlorine-doping of metal-free ceria (Section 2.1). This suggestion arises from the results of works [29–31], which proves that the formation of CeOCl phase goes up in the presence of a supported metal, which enhances hydrogen dissociation and CeO_2 reduction. In the absence of a supported metal Cl probably anchors only onto reduced surface sites, *i.e.* surface Ce^{3+}-coupled oxygen vacancies, and CeOCl phase formation becomes difficult because pure CeO_2 does not undergo reduction until *ca.* 350 °C [31] while NH_4Cl completely decomposes at 350 °C.

3.1.3. HAADF-STEM and EDX-mapping

HAADF-STEM images and EDX elemental maps were acquired for the used Ni/CeO_2, Ni(Cl*)/CeO_2 (Fig. 2) and Ni/CeO_2(Cl*) catalysts. Our attempts to identify supported Ni particles on the catalysts using HAADF-STEM and TEM (not presented) images were unsuccessful due to low contrast of Ni on ceria. For this reason we applied EDX-mapping technique to identify Ni nanoparticles in the studied samples. EDX-mapping is a useful tool for determining the catalyst elemental composition and compositional homogeneity.

Fig. 2b–d represent the Ce, Cl and Ni distribution maps of the Ni(Cl*)/CeO_2 catalyst. It is seen that Ce and Cl are almost uniformly distributed throughout the sample; the Cl and Ce distribution maps coincide thus indicating the presence of chlorine-ceria chemical interaction and probable formation of the CeOCl species. In contrast to Cl and Ce, Ni is distributed non-uniformly: it exists in a form of Ni nanoparticle agglomerates sizing within a wide range of 20–200 nm (marked by circles at Fig. 2). No similarity between Ni and Cl or Ce distribution maps is observed for Ni(Cl*)/CeO_2 catalyst. Similar results were obtained for Ni/CeO_2(Cl*) catalyst. This fact allows suggestion that no specific chemical interaction between Ni and Cl occurs and

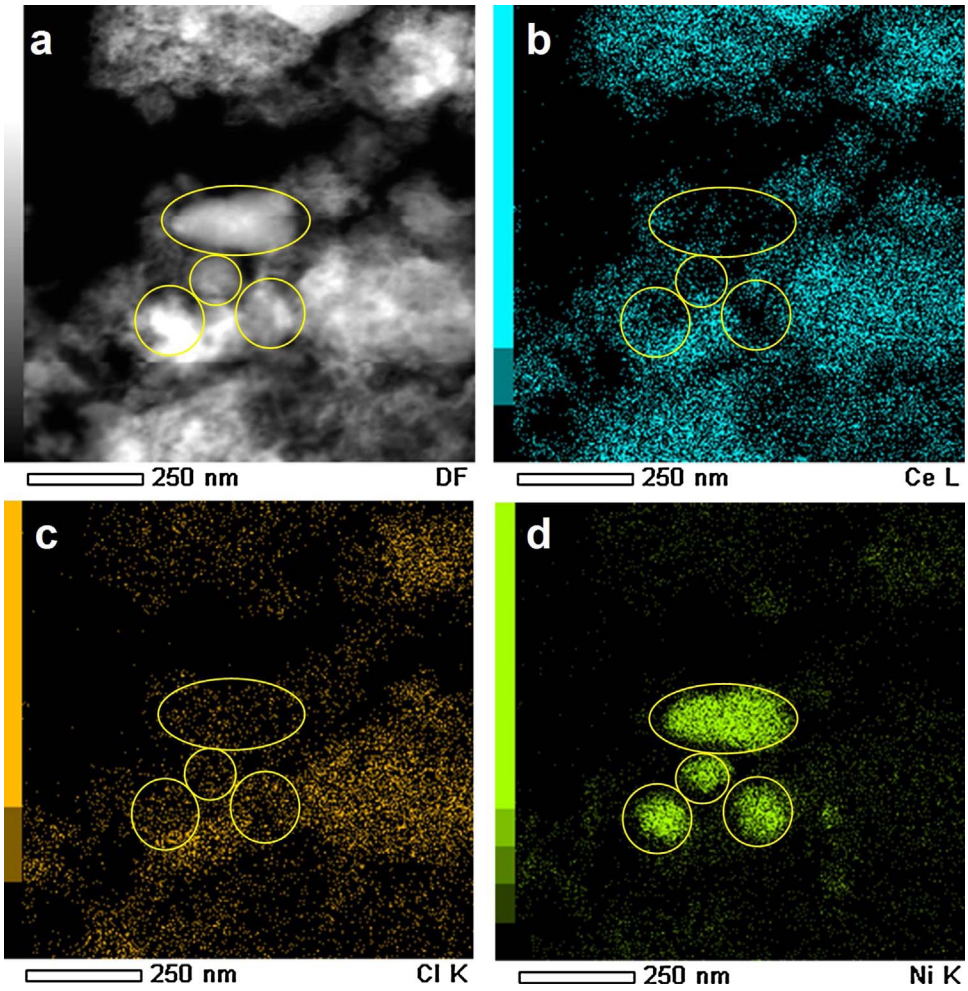

Fig. 2. HAADF-STEM image (a) and corresponding Ce (b), Cl (c) and Ni (d) distribution maps for Ni(Cl*)/CeO_2 catalyst. Circles designate the zones where Ni predominates.

chlorine is distributed predominantly over the ceria surface.

HAADF-STEM images and EDX elemental maps for Ni/CeO_2 and Ni/CeO_2(Cl*) could be found in Supplementary information. The detailed TEM and EDX analysis of Ni(Cl)/CeO_2 catalyst was performed in our previous work [19] and is not presented here.

3.1.4. XPS

The XPS analysis showed the presence of cerium, oxygen, nickel and insignificant carbon on the surface of all catalysts and additionally chlorine for Cl-containing samples. Table 3 represents the data on surface Cl/Ce and Ce^{3+}/Ce (Ce = Ce^{3+} + Ce^{4+}) atomic ratios for the catalysts. It is seen, that for all Cl-containing catalysts surface Cl/Ce atomic ratio is quite high (0.61 for Ni(Cl*)/CeO_2, 0.23 for Ni(Cl)/CeO_2 and 0.23 for Ni/CeO_2(Cl*)). For Ni(Cl*)/CeO_2 and Ni(Cl)/CeO_2 catalysts relatively high surface Cl/Ce atomic ratio is in a good agreement with high bulk Cl/Ce atomic ratio (Table 3) and the presence of CeOCl phase (Table 2). While in the case of Ni/CeO_2(Cl*) surface Cl/Ce atomic ratio (0.23) is significantly higher than bulk one (0.08) indicating that near-all chlorine is located on the catalyst surface. We associate Cl anchoring with formation of CeOCl phase or at least CeOCl-like surface species *i.e.* Ce^{3+}-containing species. It could be noted that for Ni(Cl*)/CeO_2 and Ni(Cl)/CeO_2 surface Ce^{3+}/Ce atomic ratios is higher (Table 3) than 0.2 which is a typical value for non-modified CeO_2 [18]. This fact is in a good agreement with the presence of CeOCl phase in these catalysts (Table 2). For Ni/CeO_2 and Ni/CeO_2(Cl*) surface content Ce^{3+}/Ce atomic ratio is close to 0.2. It is expectable for unpromoted ceria surface of Ni/CeO_2 and for chlorinated ceria surface of Ni/CeO_2(Cl*) because in the latter case Cl was anchored onto ceria surface with a standard degree of reduction (*i.e.* Ce^{3+}/Ce close to 0.2) in the absence of a supported metal.

The Ce3d, Ni2p and Cl2p XP-spectra of the catalysts could be found in the Supplementary information.

Table 3
XPS data for the used catalysts

Catalyst	Cl/Ce atomic ratio		Ce^{3+}/Ce surface atomic ratio[a]
	surface[a]	bulk[b]	
Ni/CeO_2	–	–	0.22
Ni(Cl*)/CeO_2	0.61	0.46	0.50
Ni(Cl)/CeO_2	0.23	0.50	0.31
Ni/CeO_2(Cl*)	0.23	0.08	0.20

[a]According to the XPS data.
[b]According to the chemical composition (Table 1).

3.1.5. Summary

The above comparative analysis of the catalyst characterization data (Section 3.1.1–3.1.4) allows the following conclusions:

i) All the catalysts contained the CeO_2 phase with average crystalline size of 9.0–9.5 nm, which is equal to crystalline size of pure CeO_2 support.

ii) The Ni loading in all the catalysts was almost the same and amounted to 8–10 wt.%. The average size of Ni particles, which were distributed in the large agglomerates, depended on the preparation procedure and increased ten-fold (from *ca.*10 to 100 nm) in the following order:

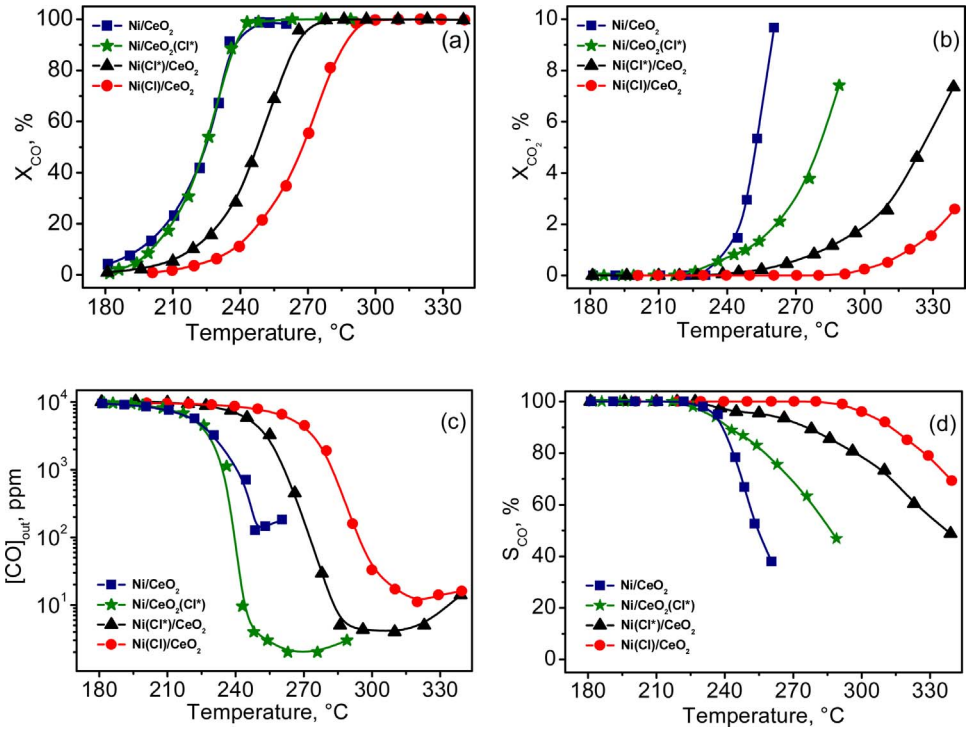

Fig. 3. The temperature dependences of X_{CO} (a), X_{CO2} (b), CO outlet concentration (c) and CO selectivity (d) for CO-SMET over the Ni/CeO_2, $Ni/CeO_2(Cl^*)$, $Ni(Cl^*)/CeO_2$, $Ni(Cl)/CeO_2$ catalysts. Feed gas composition (vol.%): 1.0 CO, 65H_2, 10H_2O, 20 CO_2 with He as balance. WHSV: 29,000 $cm^3\,g^{-1}\,h^{-1}$.

$Ni/CeO_2 \le Ni/CeO_2(Cl^*) < Ni(Cl^*)/CeO_2 < Ni(Cl)/CeO_2$

Specific surface area of Ni decreased in this raw by an order of magnitude (from 3.8 for Ni/CeO_2 to 0.5 m^2/g_{cat} for $Ni(Cl)/CeO_2$).

iii) The chlorine content in the chlorinated catalysts depended on the preparation procedure and amounted to *ca.* 8 wt.% for $Ni(Cl^*)/CeO_2$ and $Ni(Cl)/CeO_2$ and *ca.* 1.5 wt.% for $Ni/CeO_2(Cl^*)$. In those catalysts chlorine was distributed predominantly on the surface of ceria with the formation of oxychloride Ce^{3+} species in a form of stable CeOCl phase particles of size 15–19 nm and/or amorphous/well dispersed CeOCl-like surface species.

3.2. CO-SMET performance

Fig. 3 illustrates the effect of temperature on the CO and CO_2 conversions, CO outlet concentration and CO selectivity in CO-SMET for all the catalysts. It is seen that the catalysts were active in CO and CO_2 methanation and demonstrated the X_{CO} and $X_{CO_2}^{Ref}$ (Fig. 3a–d), [CO] outlet concentrations and S_{CO} temperature dependences of the same type. With increasing temperature, the CO and CO_2 conversions increased; the outlet CO concentration first decreased, reached the minimum and then increased; the CO selectivity – decreased. Note that the observed curves are similar to CO-SMET temperature dependences observed in many works [21]. It is assumed that the increase of CO outlet concentration after passing through minimum is caused by increasing contribution of the reverse water gas shift reaction, whereas the decrease in CO selectivity – by simultaneous CO_2 methanation. Let us consider the data presented in Fig. 3 in more detail.

It is seen (Fig. 3a) that the CO conversion for all catalysts increases with increasing temperature and attains ~100%. In case of Cl-free Ni/CeO_2 catalyst, the maximum X_{CO} of 98.7% was reached at ≥245 °C. All chlorinated catalysts ($Ni/CeO_2(Cl^*)$, $Ni(Cl^*)/CeO_2$, $Ni(Cl)/CeO_2$) provided $X_{CO} \ge 99.9\%$ which were reached at T ≥ 240 °C, T ≥ 285 °C, T ≈ 320 °C, respectively. The X_{CO} temperature dependences of Ni/CeO_2 and $Ni/CeO_2(Cl^*)$ were similar, while those of $Ni(Cl^*)/CeO_2$ and $Ni(Cl)/CeO_2$ were shifted towards higher temperatures. This fact means that the catalyst activity for CO methanation (calculated per catalyst weight) decreases in the following order:

$Ni/CeO_2 \ge Ni/CeO_2(Cl^*) > Ni(Cl^*)/CeO_2 > Ni(Cl)/CeO_2$

The observed trend allows suggestion that CO methanation proceeds over both Cl-free and Cl-containing Ni/CeO_2 catalysts by similar way, predominantly on the nickel surface, *via* CO and H_2 chemisorption [19,22]. If so, the trend seems quite natural, since respective Ni surface area decreases in this catalyst raw (Section 3.1.2, Table 2).

The CO_2 conversion (Fig. 3b) also increased with increasing temperature for all the catalysts and did not exceed 10% in the all studied temperature intervals. Note that at high $X_{CO_2}^{Ref}$ uncontrollable heating of the catalyst layer owing to adiabatic runaway was observed. Comparative analysis of the data presented in Fig. 3a,b shows that the $X_{CO_2}^{Ref}$ temperature dependences for all catalysts are shifted towards higher temperatures as compared to respective X_{CO} curves; methanation of CO_2 over all catalysts occurs after almost all CO is converted into methane, *i.e.* at low CO content in the outlet reaction mixture. Indeed, Ni/CeO_2 and $Ni/CeO_2(Cl^*)$ provided noticeable CO_2 conversion at T ≥ 230 °C, $Ni(Cl^*)/CeO_2$ and $Ni(Cl)/CeO_2$ at T ≥ 280 and ≥ 320 °C, respectively. This means that catalytic activity for CO_2 methanation (calculated per catalyst weight) decreases in the following order:

$Ni/CeO_2 \ge Ni/CeO_2(Cl^*) > Ni(Cl^*)/CeO_2 > Ni(Cl)/CeO_2$

This trend is similar to that of CO methanation activity. It could be explained, if under CO-SMET conditions CO inhibits CO_2 methanation.

The considered data (Fig. 3a,b) allows one to conclude, that all the catalysts are capable to perform preferential CO methanation in the presence of CO_2, although in various temperature intervals. However, compared to chlorinated catalysts, Cl-free Ni/CeO_2 appears inefficient for deep CO removal from reformate gas. As Fig. 3c,d shows, the minimum $[CO]_{out}$ over Cl-free Ni/CeO_2 was only ~130 ppm at 245–260 °C and S_{CO} ~60–35%. All Cl-containing catalysts showed much higher CO cleanup efficiency and provided CO removal from reformate gas to the level of ≤10 ppm, no matter by which method they were doped with chlorine. In particular, $[CO]_{out}$ ~ 10 ppm and S_{CO} of 90 ÷ 50% were reached (Fig. 3c,d) at 240–285 °C for $Ni/CeO_2(Cl^*)$; at 285–335 °C for $Ni(Cl^*)/CeO_2$; at 310–330 °C for $Ni(Cl)/CeO_2$. This fact agrees with the recent results [8,16,19–21] which prove positive effect of chlorine adding to Ru/Al_2O_3, Ni/TiO_2, Ni/CeO_2 and Ni

alumina based catalysts on their performance in CO-SMET.

According to [19,22], the observed effect of Cl doping for ceria supported nickel catalysts is most likely explained by the fact that the CO_2 methanation over Cl-free Ni/CeO_2 catalyst predominantly proceeds *via* CO_2 adsorption on the ceria surface (Ce^{3+} and oxygen vacancy) and stepwise hydrogenation to methane through hydrocarbonate and formate intermediates by hydrogen atoms spilled over from Ni particles. With the Cl-containing $Ni(Cl)/CeO_2$, $Ni(Cl^*)/CeO_2$ and $Ni/CeO_2(Cl^*)$ catalysts this reaction pathway is locked due to the ceria surface blockage by chlorine to inhibit CO_2 adsorption and methanation. As a result, Cl-containing catalysts demonstrate a higher CO-SMET performance as compared to Cl-free Ni/CeO_2 samples.

To verify this hypothesis, we have compared the catalysts activity in CO (TOF_{CO}) and CO_2 (TOF^{Ref}_{CO2}) methanation with respect to Ni surface atoms under realistic CO-SMET conditions, analyzed catalysts activity towards CO_2 methanation in terms of X_{CO2} and TOF_{CO2} in model mixture (1 vol.% CO_2, 65 vol.% H_2 and He-balance) and studied the nature of surface species during the CO_2 methanation by FTIR *in situ* technique. The obtained results are discussed in the next section.

3.3. Insight into chlorine doping effect on CO-SMET performance

Catalytic activity (calculated per catalyst weight) for CO methanation in the reformate gas decreases in the order $Ni/CeO_2 \geq Ni/CeO_2(Cl^*) > Ni(Cl^*)/CeO_2 > Ni(Cl)/CeO_2$ (Section 3.2). This trend is most likely attributed to the fact that specific surface of nickel decreases in the same order from 3.8 m^2/g_{cat} for Ni/CeO_2 to 0.5 m^2/g_{cat} for $Ni(Cl)/CeO_2$ (Section 3.1.2). At the same time for all the studied ceria supported nickel catalysts TOF_{CO} does not demonstrate any dependence on both the size of supported Ni particles and chlorinating procedure (Fig. 4). It is seen that TOFs of all catalysts are almost similar (the maximum difference is less than two times). Moreover, the activation energy of CO methanation over all catalysts, calculated from the slope of the plots, appeared similar and amounted to 140 ± 15 kJ/mole. This fact together with our previous data on CO methanation kinetics over Ni/CeO_2 and $Ni(Cl)/CeO_2$ catalysts [22] and literature data on mechanisms of CO methanation over Ni catalysts [32,33] could be conformed, if CO methanation proceeds predominantly over Ni surface for all studied catalysts and Cl does not influence catalyst's CO methanation activity.

The following values of TOF (TOF^{Ref}_{CO2}) were obtained for CO_2 methanation at 250 °C under realistic CO-SMET conditions: 0 for $Ni(Cl)/CeO_2$, 2×10^{-3} s^{-1} for $Ni(Cl^*)/CeO_2$, 6×10^{-3} s^{-1} for $Ni/CeO_2(Cl^*)$ and 2×10^{-2} s^{-1} for Ni/CeO_2. It is obviously seen, that TOFs differ a lot by value and rise with the decrease of Cl content in the catalysts

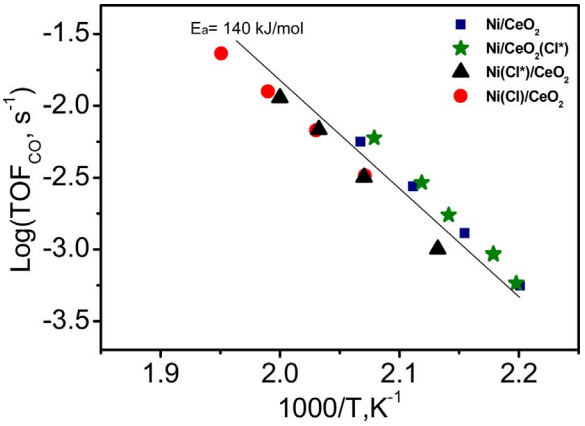

Fig. 4. Arrhenius plots of turnover frequencies of Ni surface atoms for CO methanation (TOF_{CO}) in CO-SMET over Ni/CeO_2, $Ni/CeO_2(Cl^*)$, $Ni(Cl^*)/CeO_2$, $Ni(Cl)/CeO_2$ catalysts. Feed gas composition (vol.%): 1.0 CO, 65H_2, 10H_2O, 20 CO_2 with He as balance. WHSV: 29,000 $cm^3\,g^{-1}\,h^{-1}$. CO conversion (X_{CO}) < 15% and $S_{CO} \approx 100\%$.

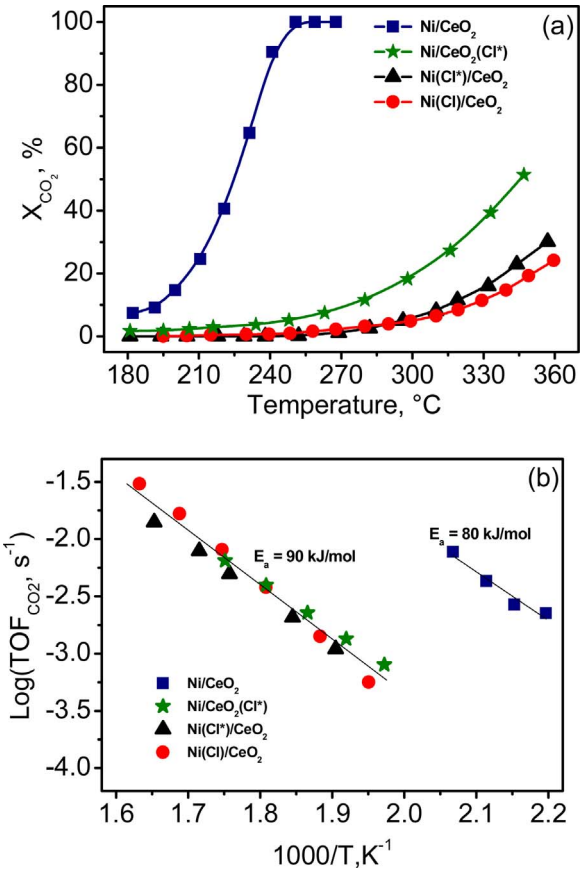

Fig. 5. The temperature dependences of X_{CO2} (a) and Arrhenius plots of turnover frequencies of Ni surface atoms (b) for the CO_2 methanation in model mixture over the Ni/CeO_2, $Ni/CeO_2(Cl^*)$, $Ni(Cl^*)/CeO_2$, $Ni(Cl)/CeO_2$ catalysts. Feed gas composition (vol.%): 1.0 CO_2, 65H_2 with He as balance. WHSV: 29,000 $cm^3g^{-1}\,h^{-1}$.

(Table 1). To emphasize the differences in catalytic activity towards CO_2 methanation between catalysts with various Cl content we performed experiments in model mixture (1 vol.% CO_2, 65 vol.% H_2 and He-balance) in the absence of CO inhibition effect. Fig. 5a illustrates the effect of temperature on the CO_2 conversions for all the catalysts. No CO was detected and CH_4 was the only product in the course of experiments, therefore CH_4-selectivity graph is not presented. It is seen (Fig. 5a) that Ni/CeO_2 is much more active providing complete CO_2 methanation already at 240 °C while Cl-containing catalysts exhibit essential activity at T ≥ 270–300 °C. Activity of Cl-containing catalysts decreases in the order $Ni/CeO_2(Cl^*) > Ni(Cl^*)/CeO_2 \geq Ni(Cl)/CeO_2$ with decrease of specific surface of nickel (Table 2) and increase of Cl content (Table 1). Consideration of TOFs for CO_2 methanation (TOF_{CO2}) in model mixture (Fig. 5b) reveals a similar activity and activation energy (90 ± 10 kJ/mole) for Cl-containing catalysts and a much higher (1.5 orders of magnitude) activity and close activation energy (80 ± 10 kJ/mol) for Ni/CeO_2. Thus, chlorine doping, does not matter how, strongly inhibits the CO_2 methanation activity and probably changes the CO_2 methanation reaction route. This will be discussed below.

The observed trends of catalysts activity towards CO_2 methanation could be explained, if CO_2 methanation over Cl-containing catalysts proceeds predominantly over Ni surface at T > 300 °C, while for Ni/CeO_2 there is a low-temperature (200–250 °C) route through CO_2 activation over CeO_2 surface, as it was discussed in [22,34–36]. This hypothesis also explains the CO inhibition effect on CO_2 methanation under realistic CO-SMET conditions: in the case of Cl-free Ni/CeO_2 catalyst CO covers Ni surface and hampers H_2 dissociation and therefore H spillover to ceria surface; in the case of Cl-containing catalysts

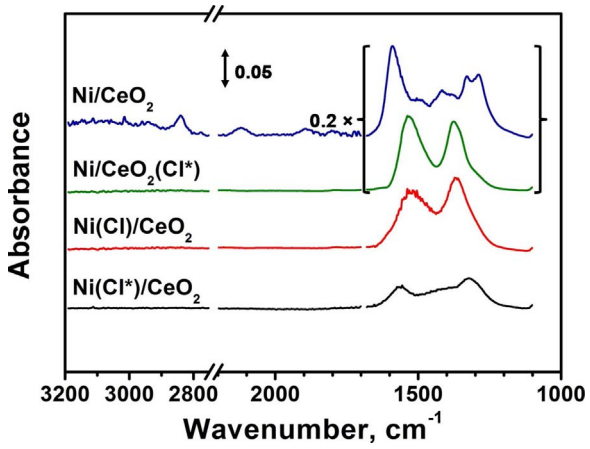

Fig. 6. *In situ* FTIR spectra at the CO_2 methanation over Ni/CeO_2, $Ni/CeO_2(Cl^*)$, $Ni(Cl^*)/CeO_2$, $Ni(Cl)/CeO_2$ catalysts at 250 °C. Flow rate 168,000 $cm^3\ g^{-1}\ h^{-1}$. Feed gas composition (vol.%): 1 CO_2 + 65H_2 + He-balance.

CO adsorption inhibits CO_2 and H_2 adsorption onto Ni surface.

To clarify the nature of surface species during the CO_2 methanation in a model mixture (1 vol.% CO_2, 65 vol.% H_2 and He-balance) we have performed FTIR *in situ* experiments. Fig. 6 represents IR-spectra of Ni/CeO_2, $Ni/CeO_2(Cl^*)$, $Ni(Cl)/CeO_2$ and $Ni(Cl^*)/CeO_2$ during the CO_2 methanation at 250 °C ($X_{CO2} \leq 30\%$). The spectrum of CO_2 on Ni/CeO_2 contains absorption bands assigned to bridged (1800–1900 cm^{-1}) Ni carbonyls; terminal CO (2117 cm^{-1}), most likely, on the support surface; monodentate (1370, 1480–1530 cm^{-1}) and bidentate (1290, 1574 cm^{-1}) carbonates; hydrocarbonates (1417, 1592 cm^{-1}) and formates (1330, 2841 cm^{-1}) on the surface of CeO_2. The IR-spectrum of Ni/CeO_2 also contains the gaseous methane absorption band at 3015 cm^{-1} confirming the catalyst activity in CO_2 methanation. Data from [35–37] were used for bands assignment. The presence of hydrocarbonates and formates indicates the occurrence of CO_2 methanation through the formate route [22,34–36] over Ni/CeO_2 catalyst. In the same time, the IR-spectra of Cl-containing catalysts are much poorer and essentially contain two absorption bands at 1330–1370 and 1530–1560 cm^{-1} which could be assigned to monodentate carbonates adsorbed on the support surface. The two main observations could be done considering the spectra of Cl-containing catalysts:

i) The higher is the Cl content the weaker is carbonate bands intensity. The latter is *ca.* 12 times less intensive for $Ni(Cl^*)/CeO_2$ and *ca.* 5 times less intensive for $Ni(Cl)/CeO_2$ than for $Ni/CeO_2(Cl^*)$. Thus, Cl doping strongly changes ceria surface chemistry suppressing CO_2 adsorption.
ii) For all Cl-containing catalysts no bands related to formates or hydrocarbonates are detected, even at high temperatures (See Fig. S7 in Supplementary information), indicating the complete inhibition of CO_2-derived species hydrogenation by chlorine. And this is why does chlorine doping promote the CO-SMET performance of nickel-ceria catalysts.

According to the recent paper [36] on the mechanism of the CO_2 methanation over Ru/CeO_2 catalyst Ce^{3+} surface sites can act as a Lewis base sites and are of key importance for CO_2 activation. The important role of Ce^{3+} surface sites in CO_2 adsorption was also noted in the review paper [38]. So it is obvious that when Ce^{3+} surface sites are locked by chlorine, CeO_2 surface is not able to activate CO_2. This works even in the case of $Ni/CeO_2(Cl^*)$ with low chlorine content, because Ce^{3+} surface sites are still occupied by Cl atoms. Thus, we consider Ce^{3+} surface sites locking with the formation of CeOCl-like species to be the origin of chlorine doping effect on the CO-SMET performance of the nickel-ceria catalysts.

The treatment of ceria surface by NH_4Cl provides a great tool to tune the properties of nickel-ceria catalysts in CO-SMET inhibiting the CO_2 methanation activity. The CeO_2 treatment before Ni deposition seems to be the most promising approach which provides only surface modification of ceria with blockage of Ce^{3+} surface sites and high nickel dispersion. The catalyst activity and selectivity could be further improved by optimizing the NH_4Cl treatment procedure and studying other chlorinating agents.

4. Conclusion

Selective CO methanation (CO-SMET) in the reformate gas was investigated over nickel-ceria catalysts prepared by impregnating: CeO_2 with Ni(II) nitrate and Ni(II) chloride, Ni/CeO_2 – with NH_4Cl, CeO_2 – with NH_4Cl followed by Ni depositing. It was shown that all Cl-containing Ni/CeO_2 catalysts provided efficient CO cleanup. In particular, they provided the removal of CO from reformate gas to the level below 10 ppm with a selectivity of up to 90%. The advanced performance of Cl-containing catalysts was associated with the inhibition of undesirable side reaction of CO_2 methanation, that was confirmed by CO_2 methanation experiments and FTIR *in situ*. The catalyst characterization by BET, XRD, XPS, HAADF-STEM, EDX-mapping and CO chemisorption techniques revealed that the decrease in chlorine content in raw $Ni(Cl)/CeO_2 \geq Ni(Cl^*)/CeO_2 > Ni/CeO_2(Cl^*)$ was accompanied by the increase in Ni dispersion that most likely provided high performance of $Ni/CeO_2(Cl^*)$ in CO-SMET. The turnover frequencies of Ni surface atoms as well as activation energies in CO methanation were practically similar for all studied catalysts, indicating that CO methanation proceeded by similar ways over Ni surface in both Cl-free and Cl-containing samples. The chlorine doping effect was attributed to the blockage of surface Ce^{3+}-coupled oxygen vacancy sites by CeOCl species that inhibited ceria-assisted CO_2 activation and hydrogenation. The CeO_2 treatment with NH_4Cl before Ni deposition allows to prepare highly active and selective CO-SMET catalyst with high nickel dispersion and Cl-modified ceria surface.

Acknowledgements

The authors are grateful to Dr. V.P. Pakharukova for assistance in XRD analysis and Dr. R.V. Gulyaev for assistance in XPS analysis.

This work is conducted within the framework of budget project No. 0303-2016-0011 for Boreskov Institute of Catalysis. D.I. Potemkin appreciate financial support from Russian Federation President's scholarship SP-922.2016.1.

Appendix A. Supplementary data

Supplementary data associated with this article can be found, in the online version, at http://dx.doi.org/10.1016/j.apcatb.2017.09.038.

References

[1] S.J. Peighambardoust, S. Rowshanzamir, M. Amjadi, Review of the proton exchange membranes for fuel cell applications, Int. J. Hydrogen Energy 35 (2010) 9349–9384.
[2] V. Mehta, J.S. Cooper, Review and analysis of PEM fuel cell design and manufacturing, J. Power Sources 114 (2003) 32–53.
[3] E.D. Park, D. Lee, H.C. Lee, Recent progress in selective CO removal in a H_2-rich stream, Catal. Today 139 (2009) 280–290.
[4] M.A. Ashraf, G. Ercolino, S. Specchia, V. Specchia, Final step for CO syngas clean–up: comparison between CO-PROX and CO-SMET processes, Int. J. Hydrogen Energy 39 (2014) 18109–18119.
[5] P. Panagiotopoulou, D.I. Kondarides, X.E. Verykios, Mechanistic study of the selective methanation of CO over Ru/TiO_2 catalyst: identification of active surface species and reaction pathways, J. Phys. Chem. C 115 (2010) 1220–1230.
[6] S. Takenaka, T. Shimizu, K. Otsuka, Complete removal of carbon monoxide in hydrogen–rich gas stream through methanation over supported metal catalysts, Int. J. Hydrogen Energy 29 (2004) 1065–1073.
[7] S. Eckle, Y. Denkwitz, R.J. Behm, Activity, selectivity, and adsorbed reaction intermediates/reaction side products in the selective methanation of CO in reformate

gases on supported Ru catalysts, J. Catal. 269 (2010) 255–268.
[8] P. Djinović, C. Galletti, S. Specchia, V. Specchia, CO methanation over Ru–Al_2O_3 catalysts: effects of chloride doping on reaction activity and selectivity, Top. Catal. 54 (2011) 1042–1053.
[9] R.A. Dagle, Y. Wang, G.G. Xia, J.J. Strohm, J. Holladay, D.R. Palo, Selective CO methanation catalysts for fuel processing applications, Appl. Catal. A: Gen. 326 (2007) 213–218.
[10] S. Tada, R. Kikuchi, Preparation of Ru nanoparticles on TiO_2 using selective deposition method and their application to selective CO methanation, Catal. Sci. Technol. 4 (2014) 26–29.
[11] Z. Kowalczyk, K. Stołecki, W. Rarog-Pilecka, E. Miśkiewicz, E. Wilczkowska, Z. Karpiński, Supported ruthenium catalysts for selective methanation of carbon oxides at very low CO_X/H_2 ratios, Appl. Catal. A: Gen. 342 (2008) 35–39.
[12] P. Panagiotopoulou, D.I. Kondarides, X.E. Verykios, Selective methanation of CO over supported Ru catalysts, Appl. Catal. B: Environ. 88 (2009) 470–478.
[13] P. Panagiotopoulou, D.I. Kondarides, X.E. Verykios, Selective methanation of CO over supported noble metal catalysts: effects of the nature of the metallic phase on catalytic performance, Appl. Catal. A: Gen. 344 (2008) 45–54.
[14] K. Urasaki, K.I. Endo, T. Takahiro, R. Kikuchi, T. Kojima, S. Satokawa, Effect of support materials on the selective methanation of CO over Ru catalysts, Top. Catal. 53 (2010) 707–711.
[15] H. Yoshida, K. Watanabe, N. Iwasa, S.I. Fujita, M. Arai, Selective methanation of CO in H_2-rich gas stream by synthetic nickel–containing smectite based catalysts, Appl. Catal. B: Environ. 162 (2015) 93–97.
[16] T. Miyao, W. Shen, A. Chen, K. Higashiyama, M. Watanabe, Mechanistic study of the effect of chlorine on selective CO methanation over Ni alumina–based catalysts, Appl. Catal. A: Gen. 486 (2014) 187–192.
[17] M.M. Zyryanova, P.V. Snytnikov, Yu.I. Amosov, S.A. Ven', yaminov, E.Z. Golosman, V.A. Sobyanin, Selective methanation of CO in the presence of CO_2 in hydrogen-containing mixtures on nickel catalysts, Kinet. Catal. 51 (2010) 907–913.
[18] M.M. Zyryanova, P.V. Snytnikov, R.V. Gulyaev, Yu.I. Amosov, A.I. Boronin, V.A. Sobyanin, Performance of Ni/CeO_2 catalysts for selective CO methanation in hydrogen-rich gas, Chem. Eng. J. 238 (2014) 189–197.
[19] M.V. Konishcheva, D.I. Potemkin, P.V. Snytnikov, M.M. Zyryanova, V.P. Pakharukova, P.A. Simonov, V.A. Soobyanin, Selective CO methanation in H_2-rich stream over Ni-, Co- and Fe/CeO_2: effect of metal and precursor nature, Int. J. Hydrogen Energy 40 (2015) 14058–14063.
[20] N. Shimoda, D. Shoji, K. Tani, M. Fujiwara, K. Urasaki, R. Kikuchi, S. Satokawa, Role of trace chlorine in Ni/TiO_2 catalyst for CO selective methanation in reformate gas, Appl. Catal. B: Environ. 174 (2015) 486–495.
[21] P.V. Snytnikov, M.M. Zyryanova, V.A. Sobyanin, CO-cleanup of hydrogen-rich stream for LT PEM FC feeding: catalysts and their performance in selective CO methanation, Top. Catal. 59 (2016) 1394–1412.
[22] M.V. Konishcheva, D.I. Potemkin, S.D. Badmaev, P.V. Snytnikov, E.A. Paukshtis, V.A. Sobyanin, V.N. Parmon, On the mechanism of CO and CO_2 methanation over Ni/CeO_2 catalysts, Top. Catal. 59 (2016) 1424–1430.
[23] P.A. Kilty, W.M.H. Sachtler, The mechanism of the selective oxidation of ethylene to ethylene oxide, Catal. Rev. 10 (1) (1974) 1–16.
[24] S. Linic, M.A. Barteau, Heterogeneous catalysis of alkene epoxidation, in: H. Ertl, F. Knoezinger (Eds.), Handbook of Heterogeneous Catalysis, Wiley-VCH, Weinheim, 2008, pp. 3448–3464.
[25] N.I. Petrova, D.Yu. Troitskii, I.I. Novoselov, A.I. Saprykin, Determination of chlorine in bismuth and bismuth oxide by atomic absorption spectrometry and laser mass spectrometry, Inorg. Mater. 51 (2015) 559–562.
[26] G. Bergeret, P. Gallezot, Particle size and dispersion measurements, in: H. Ertl, F. Knoezinger (Eds.), Handbook of Heterogeneous Catalysis, Wiley-VCH, Weinheim, 2008, pp. 738–765.
[27] F. Le Normand, J. Barrault, R. Breault, L. Hilaire, A. Kiennemann, Catalysis with palladium deposited on rare earth oxides: influence of the support on reforming and syngas activity and selectivity, J. Phys. Chem. 95 (1991) 257–269.
[28] S. Bernal, F.J. Botana, J.J. Calvino, G.A. Cifredo, J.P. Omil, HREM study of the phases resulting from the preparation of ceria supported rhodium catalysts, Electron Microsc. Anal. 138 (1993) 485–488.
[29] L. Kepiński, M. Wołcyrz, J. Okal, Effect of chlorine on microstructure and activity of Pd/CeO_2 catalysts, J. Chem. Soc. Faraday Trans. 91 (1995) 507–515.
[30] D.I. Kondarides, X.E. Verykios, Effect of chlorine on the chemisorptive properties of Rh/CeO_2 catalysts studied by XPS and temperature programmed desorption techniques, J. Catal. 174 (1998) 52–64.
[31] F. Fajardie, J.M. Manoli, G. Djega-Mariadassou, G. Blanchard, Ceria lattice oxygen ion substitution by Cl–during the reduction of Rh (Cl)/CeO_2 catalysts. Formation and stability of CeOCl, J. Chem. Soc. Faraday Trans. 94 (1998) 3727–3735.
[32] J. Sehested, S. Dahl, J. Jacobsen, J.R. Rostrup-Nielsen, Methanation of CO over nickel: mechanism and kinetics at high H_2/CO ratios, J. Phys. Chem. B 109 (2005) 2432–2438.
[33] D.W. Goodman, R.D. Kelley, T.E. Madey, J.T. Yates, Kinetics of the hydrogenation of CO over a single crystal nickel catalyst, J. Catal. 63 (1980) 226–234.
[34] P.A. Ussa Aldana, F. Ocampo, K. Kobl, B. Louis, F. Thibault-Starzyk, M. Daturi, P. Bazin, S. Thomas, A.C. Roger, Catalytic CO_2 valorization into CH_4 on Ni-based ceria-zirconia. Reaction mechanism by operando IR spectroscopy, Catal. Today 215 (2013) 201–207.
[35] Q. Pan, J. Peng, S. Wang, S. Wang, In situ FTIR spectroscopic study of the CO_2 methanation mechanism on Ni/$Ce_{0.5}Zr_{0.5}O_2$, Catal. Sci. Technol. 4 (2014) 502–509.
[36] F. Wang, S. He, H. Chen, B. Wang, L. Zheng, M. Wei, D.G. Evans, X. Duan, Active site dependent reaction mechanism over Ru/CeO_2 catalyst toward CO_2 methanation, J. Am. Chem. Soc. 138 (2016) 6298–6305.
[37] G.N. Vayssilov, M. Mihaylov, P.S. Petkov, K.I. Hadjiivanov, K.M. Neyman, Reassignment of the vibrational spectra of carbonates, formates, and related surface species on ceria: a combined density functional and infrared spectroscopy investigation, J. Phys. Chem. C 115 (2011) 23435–23454.
[38] D.R. Mullins, The surface chemistry of cerium oxide, Surf. Sci. Rep. 70 (2015) 42–85.